Investigation of the High-pressure Behaviour of Clinochlore by X-ray Diffraction and

Infrared Spectroscopy

Bingxu Hou^{1,2}, Jingjing Niu³, Lili Zhang⁴, Hongrui Ding^{1,2}, Shan Qin¹, Anhuai Lu^{1,2},

Hongyan Zuo^{5,*}

¹SKLab-DeepMinE, MOEKLab-OBCE, School of Earth and Space Sciences, Peking

University, Beijing 100871, China

²Beijing Key Laboratory of Mineral Environmental Function, School of Earth and Space

Sciences, Peking University, Beijing 100871, China

³Center for High Pressure Science and Technology Advanced Research, Beijing 100094,

China

⁴Shanghai Synchrotron Radiation Facility, Shanghai Advanced Research Institute, Chinese

Academy of Sciences, Shanghai 201204, China

⁵State Key Laboratory of Lunar and Planetary Sciences, Macau University of Science and

Technology, Macau 999078, China

*Corresponding author: Hongyan Zuo (hyzuo@must.edu.mo)

Abstract

Chlorite plays an essential role in transporting water into the deep Earth. This study

investigates the high-pressure behaviour of clinochlore up to ~20 GPa at room temperature,

using synchrotron X-ray diffraction and infrared spectroscopy. We identified a polytypic

phase transition (from IIb-2 to IIa-1) at ~9 GPa and a structural distortion at ~12 GPa. The

polytypic phase transition at ~9 GPa is characterised by a significant reorganization of

interlayer hydrogen bonding, transitioning to states of weakly bonded

non-hydrogen-bonded hydroxyl groups. The phase transition showed reversibility during the

experiment. The structural distortion near 12 GPa indicates adjustments in the compression

mechanism related to the hydroxyl groups across both the brucite-like and 2:1 sheets. The

unit-cell volume of the low-pressure IIb-2 phase was fitted to the second-order

Birch-Murnaghan equation of state, and the resulting parameters are $V_0 = 710.9(3) \text{ Å}^3$ and K_0

= 83.4(8) GPa. Our results exhibit a marked deviation from prior experimental findings, potentially attribu22 to the presence of Fe²⁺ cation incorporation in the natural chlorite investigated in this work. This study emphasise the complexity of hydroxyl group in response to pressure in layered-structure silicates.

Keywords: chlorite; phase transition; high pressure; X-ray diffraction; infrared spectra

Introduction

Chlorite, as one of the most hydroxyl-rich silicates, plays an essential role in the hydrated sections of the oceanic crust and has been hypothesized to function as a major water carrier in cold subduction zones (Peacock, 1990). It was confirmed that chlorite remains stable even under high-pressure conditions exceeding 4 GPa (Fumagalli & Poli, 2005; Schmidt & Poli, 1998), highlighting its capability to contribute significantly to the water supply deep within the Earth. Particularly, Mg-rich clinochlore has been identified as the predominant aluminous phase in low-alkali hydrous peridotites at temperatures below 800°C (Jenkins, 1981). The retention of structural OH groups and H₂O within these minerals is vital for understanding their contributions to geochemical cycles and the mechanical properties of subduction zones. Thus, the study of chlorite's properties and behaviours under various pressure and temperature conditions is crucial for elucidating water transport and storage mechanisms in subduction zones, which significantly affect the rheology and seismicity of the mantle.

Clinochlore comprises two distinct polyhedral units: a brucite-like (B) layer formed of [MgO₆] octahedra, and a talc-like (TOT or 2:1) layer consisting of two tetrahedral (T) sheets sandwiching an octahedral sheet of [MgO₄(OH)₂] (Fig. 1). This structural organization provides a model for studying the response of hydroxyl groups in the layer-structure silicate to external pressures in subduction zones. The general formula for clinochlore group minerals is $(Mg,Fe,Al)_{5-6}(Si,Al)_4O_{10}(OH)_8$, with diversity in composition. The Mg-rich clinochlore is the most thermally stable and abundant mineral of the group, which can also incorporate a significant amount of Fe^{2+} in the end-member chamosite. Particularly, Brown and Bailey (1962) identified twelve chlorite polytypes that arise from various stacking configurations of the TOT and B layers. These configurations differ by translations and reversals of the slant direction of the octahedral sheets within the polyhedral layers (Brown & Bailey, 1962). Of these, the monoclinic II*b*-2 (C2/m) and triclinic II*b*-4 ($C\overline{1}$) are the two most common

polytypes in nature.

Considerable research has been conducted on the high-pressure behaviour of chlorite, yet controversies persist regarding its phase transition under high pressures. Single-crystal studies conducted within a pressure range of 10⁻⁴–5.4 GPa revealed no significant structural changes in chlorite (Zanazzi et al., 2006, 2007). However, neutron diffraction experiments up to 5 GPa (Welch & Marshall, 2001) showed that while pressure does not enhance the strength of hydrogen bonds in clinochlore, it significantly narrows O-H···O angles from 170° to 155° as well as reduces O-O distances. Extrapolating the data from Welch and Marshall (2001) to higher pressures suggests that around 8 GPa, the O-O contact distance reaches a critical point of 2.7 Å, potentially leading to anomalous structural behaviour. Meanwhile, high-pressure Raman spectroscopy conducted by Kleppe et al. (2003) identified an abrupt and significant increase in $\delta v/\delta P$ ratio for the hydrogen-bonded OH groups ($\Delta v > 120~{\rm cm}^{-1}$) at pressures between 9 and 10 GPa, suggesting a substantial reorganization of interlayer hydrogen bonding (Kleppe et al., 2003). Welch et al. (2004) employed powder synchrotron X-ray diffraction (XRD) to study synthetic clinochlore, reporting a phase transition to a more compressible structure at 9-10 GPa (Welch et al., 2004). In conjunction with Raman spectroscopy data from Kleppe et al. (2003), it was proposed that this transition was probably due to a distortion in the low-pressure IIb polytype, driven by unconventional behaviour in the interlayer hydrogen bonding rather than a polytypic phase transition. Whereas the recent single-crystal XRD study of clinochlore up to ~20 GPa indicates a polytypic phase transition from IIb-4 to IIa-1 (Soldavini et al., 2024). Overall, the high-pressure phase transition and the behaviour of hydrogen bonding and hydroxyl groups remain a subject of debate. For a deeper understanding of the structural variation underlying this behaviour, further high-pressure XRD and spectroscopic studies are necessary.

Our investigation into clinochlore is motivated not only by its potential role in transport water into the upper mantle but also by the fundamental physical processes affecting hydroxyl groups under pressure. To fully comprehend the characteristics of hydrogen bonding in minerals under deep-Earth conditions, it is essential to integrate spectroscopic data with direct structural data obtained from diffraction experiments at high pressures. Infrared (IR) spectroscopy serves as a critical tool for studying the arrangement of hydroxyl

groups within mineral structures. However, high-pressure IR spectroscopic data have not yet been reported. Therefore, we have conducted high-pressure XRD and micro-IR spectroscopy on clinochlore in a diamond anvil cell (DAC) up to approximately 20 GPa at 300 K, to elucidate the effects of pressure on chlorite structure and hydroxyl groups.

Materials and methods

Sample characterization and preparation

The sample of II*b*-2 type clinochlore was supplied by the Geological Museum of Peking University. Powder X-ray diffraction (PXRD) measurements at ambient condition were performed at the Analytical Instrumentation Center of Peking University (AIC-PKU). The experiment was conducted using PANalytical X'Pert³ Powder diffractometer equipped with a Cu K α radiation source (λ =1.5406 Å). Diffraction data were collected over the 2 θ range of 3–70° with a step size of 0.02° and a total acquisition time of 10 minutes (Fig. S1). The determined unit-cell parameters are: a=5.362(1) Å, b=9.258(2) Å, c=14.428(1) Å, β =96.970(17)°, and V=710.9(3) Å³ (space group C2/m).

The bulk composition of clinochlore was obtained using an Inductively Coupled Plasma Optical Emission Spectrometer (ICP-OES, Agilent 720ES) at AIC-PKU. Prior to the measurement, approximately 100 mg of clinochlore powder was subjected to acid digestion using nitric acid (HNO₃) in Teflon beakers under controlled heating at 80 °C for 12 hours. The resulting solution was diluted with deionized water to fixed volume and filtered to remove any undissolved residues. The prepared solutions were introduced into the plasma via a concentric nebulizer operated at a sample uptake rate of 1.0 mL·min⁻¹. The plasma power was set to 1.2 kW. Emission intensities were measured at the characteristic wavelengths (e.g., Mg: 279.553 nm, 285.213 nm; Fe: 239.563 nm, 259.940 nm; Al: 308.215 nm, 394.401 nm, 396.152 nm; Si: 250.690 nm, 251.611 nm, 288.158 nm) (Table S1). Calibration was performed using multi-element standard solutions with concentrations of 0.5, 1.0, 5.0, and 10.0 mg·L⁻¹, and a blank solution to ensure accurate background correction. Internal standards (Sc, Y) were used to monitor and correct for instrumental drift. The obtained elemental concentrations were converted to molar proportions and normalized accordingly, ensuring charge balance and consistency with the known structural framework of clinochlore. The stoichiometry of the sample is given as $(Mg_{3.18}Fe^{2+}_{1.74}Al_{1.07})(Si_{2.56}Al_{1.44})O_{10}(OH)_8$.

Prior to the high-pressure experiments, the sample was finely ground in the agate mortar and then heated at 120°C in a constant temperature furnace for 24 h to remove absorbed water. In the high-pressure XRD and IR experiments, compacted clinochlore powder was mounted in a symmetric-type DAC together with two ruby balls for pressure calibration. Culets with 400 µm in diameter and a stainless steel gasket preindented to 50 µm with a 200 µm hole were used. Clinochlore itself was used as the pressure-transmitting medium. The pressure was determined by the R1 fluorescence peak of ruby (Mao et al., 1986).

High-pressure XRD experiments

High-pressure XRD experiments were conducted at the beamline 15U in Shanghai Synchrotron Radiation Facility (SSRF). The radiation spot size on the sample was $< 3\times4~\mu\text{m}^2$ in SSRF with wavelength $\lambda = 0.6199$ Å. The distance between the sample and the detector was calibrated using a CeO₂ standard for all runs. Two-dimensional images were processed using Dioptas software (Prescher & Prakapenka, 2015) to obtain the one-dimensional diffraction spectra. The powder diffraction patterns were analysed using the Rietveld method (Rietveld, 1969) using the General Structure Analysis System (GSAS) program as implemented in the EXPGUI package (Toby, 2001).

High-pressure IR experiments

High-pressure infrared spectra were recorded at infrared beamline BL01B of Hefei Light Source (HLS). The IR radiation is extracted from a bending magnet with a superior acceptance angle of 65 mrad × 55 mrad (H × V) and high flux of approximately 10¹³ photons s⁻¹. An advanced Bruker 70v FTIR spectrometer (Bruker Corporation, Ettlingen, Germany) with a KBr beam-splitter and various detectors (a liquid-nitrogen-cooled MCT detector was used here) is available at this IR endstation. Coupled with an infrared Bruker Hyperion 3000 microscope, it covers a broad range of 650–4000 cm⁻¹ and a high spectral resolution of 0.25 cm⁻¹ for IR spectroscopy measurements at the micrometre scale.

Results

High-pressure X-ray diffraction of clinochlore

High-pressure synchrotron XRD investigations on clinochlore reveal a polytypic phase transition at ~9 GPa (from II*b*-2 to II*a*-1, with space group *C*2/*m* unchanged) based on diffraction patterns as pressure increases (Fig. 2). Notably, major differences are observed in

the 2θ range of $13-16^\circ$ (d = 2.74-2.23 Å, $\lambda = 0.6199$ Å) and involve reflections that are very sensitive to small amounts of shear of β (Fig. 2): the diffraction pattern of low-pressure IIb-type structure displays five distinct and well-resolved diffraction peaks ((114), (131)+(20 $\overline{2}$), (13 $\overline{2}$)+(201), (132)+(20 $\overline{3}$), and (13 $\overline{3}$)+(202)) (Fig. 2a); whereas the diffraction pattern of the high-pressure IIa-type structure at this range is characterized by only three broader peaks ((13 $\overline{1}$)+(200), (13 $\overline{2}$)+(201), (132)+(20 $\overline{3}$)) (Fig. 2b). Furthermore, we observe a coherent transition sequence across the pressure range: from a pure IIb-type pattern at low pressures, through a mixed-phase regime, to a dominant IIa-type pattern above 9 GPa. The high-pressure structure is consistent with the single-crystal observations reported by Soldavini et al. (2024), who identified a similar transition from triclinic IIb-4 to monoclinic IIa-1 under pressure.

The weakening of diffraction peak intensity and broadening of the full width at half maximum (FWHM) in the IIa-1 phase suggest potential amorphization at pressures above 19 GPa (Fig. 2b). The pressure dependence of key d-spacing is detailed in Fig. 3. The d_{002} spacing at ~ 7.09 Å ($2\theta \sim 5^{\circ}$) provides the most precisely determined index of the interlayer contraction, and the d_{331} spacing at ~1.54 Å (20 ~ 23°) is a sensitive index of the deformation of a and b lattice parameters (Welch et al., 2004). Also, the $d^*_{331} \wedge d^*_{001}$ angle is almost perpendicular (84°), thus, d_{331}^{-} is largely insensitive to contraction perpendicular to the structural layering. Fig. 3a clearly shows the specific impact on the d_{002} spacing, exhibiting an abrupt decrease of approximately 0.214 Å from 9.1 GPa to 12.2 GPa (0.025 Å/GPa below 9.1 GPa; 0.069 Å/GPa at 9.1 GPa-12.2 GPa). In contrast, the $d_{33\overline{1}}$ spacing decreases smoothly through the polytypic phase transition without abrupt dropping (Fig. 3b). Above 12.2 GPa, the pressure-induced reduction of the d_{002} spacing becomes significantly less pronounced, decreasing from 0.069 Å/GPa to 0.016 Å/GPa (Fig. 3a). The d_{331} spacing remains constant at ~1.495 Å (Fig. 3b). Diffraction patterns collected at the start and end of the experiment show identical peak positions (Fig. S2), which confirms the reversibility of the transformation (Kleppe et al., 2003; Soldavini et al., 2024).

Structural parameters and BM-EoS of clinochlore

Fig. 4 and Table 1 show the relative variation of unit-cell parameters derived from high-pressure experiments on clinochlore. The unit-cell parameters begin to deviate

significantly from linear behaviour around 9 GPa. As shown in Fig. 4, the a and b parameters show a nearly smooth and continuous trend with increasing pressures, whereas the c parameter, which aligns perpendicular to the layering, displays an abrupt and discontinuous decrease during the compression process. The unit-cell volume also exhibits considerable variation, decreasing from V = 659.2(1) Å³ to V = 643.6(2) Å³ as pressure increases from 7.5 to 9.1 GPa. A small increase in the β angle could also be observed (96.65° at 7.5 GPa and 97.11° at 9.1 GPa) across the phase transition. According to the chlorite structural configuration, this small variation in β angle may be associated with a rotation/translation of the superimposing layers. Above 10 GPa, the β angle stabilises at approximately 97.2° (Table 1), maintaining this value up to ~20 GPa across the entire pressure range studied.

Pressure-volume data (Fig. 4d) can be fitted with the Birch-Murnaghan equation of state (BM-EoS) (Birch, 1947) with EosFit7 software (Gonzalez-Platas et al., 2016) up to 9 GPa, while the data collected at > 9 GPa couldn't be fitted because of the complicated structural distortion according to the change in $d_{33\overline{1}}$ and d_{002} . A second-order fit gives $V_0 = 710.9(3)$ Å³, $K_0 = 83.4(8)$. These values are consistent with those reported in previous studies on chlorite using both second-order ($K_1 = 4$) and third-order BM-EoS (Table 2). The bulk modulus (K_0) of the high-pressure phase (Πa -1) shows a significant decrease of approximately 40%, indicating the substantial changes of the compressibility after the phase transition.

IR spectroscopy of clinochlore at ambient and high-pressure conditions

Infrared spectroscopy of clinochlore at ambient conditions aligns well with previous studies on chlorite (Kloprogge & Frost, 2000; Welch et al., 1995; Yang et al., 2018). The IR spectrum is characterised by a series of vibration modes of Si-O and O-H ranging from 600 to 1100 cm⁻¹, and stretching modes of O-H spanning from 3400 to 3700 cm⁻¹, as shown in Fig. S3 and Table S2. Specifically, the OH-stretching bands between 3400 and 3600 cm⁻¹ are attributed to hydrogen-bonded interlayer OH (Prieto et al., 1991; Serratosa & Vinas, 1964; Shirozu, 1980). For instance, the 3407 cm⁻¹ mode arises from OH-stretching vibrations of (SiAl)O···O-H, while the band at 3572 cm⁻¹ is associated with OH-stretching vibrations of (AlAl)O···O-H. The highest frequency of OH band at 3659 cm⁻¹, identical to the frequency of the talc OH band, is assigned to the non-hydrogen-bonded hydroxyl groups of the talc-like

2:1 layer (Inner O-H stretch). Al substitution for Mg and Fe typically results in shifts of OH stretching modes toward lower frequencies, which are influenced both by direct chemical effects on bond strength and by charge compensation through vacancies in dioctahedral clusters of the octahedral layer, thereby strengthening OH bonding (Velde, 1980).

Under high-pressure conditions, all observed modes in the 600–1100 cm⁻¹ region exhibit a positive, continuous linear pressure dependence only up to approximately 9 GPa, except the 669 cm⁻¹ mode continuously shifts up to about 20 GPa (Fig. 5a & Fig. 6a). Fig. 5b & Fig. 6b details the high-pressure evolution of the IR spectra of clinochlore in the OH-stretching region, showing that the pressure dependence of all OH modes remain linear below ~9 GPa. Near 9 GPa, significant changes occur in the frequencies of all hydrogen-bonded OH modes: notably, the 3407 cm⁻¹ hydroxyl vibration mode ((SiAl)O···O-H stretch) disappears (Fig. 5b), and the 3572 cm⁻¹ ((AlAl)O···O-H stretch) and 3659 cm⁻¹ (Inner O-H stretch) modes exhibit accelerated shifts upon compression (Fig. 6b). As the pressure continues to rise, reaching around 12 GPa, the shifting rates of frequency for these two modes begin to decelerate, eventually stabilizing into a plateau around 3658 and 3717 cm⁻¹, respectively (Fig. 5b). Upon decompression, all lattice modes and OH-stretching modes revert to their initial ambient positions (Fig. S4). Changes in both half-widths and intensities of lattice modes are reversible. The intensity of OH-stretching modes after decompression is lower than at the beginning.

Discussions

Structure evolution of clinochlore at high pressures

The changes in XRD patterns and IR vibrational spectra with pressure indicate that clinochore undergoes a polytypic phase transition at ~9 GPa and structural distortion at ~12 GPa. Above ~9 GPa, the behaviour of the vibration modes becomes more complicated, revealing the considerable complexity of hydrogen bonding in clinochlore under high-pressure conditions. Here, we discuss the specific characteristics and mechanisms of the phase transition and the structural distortion, respectively.

Polytypic phase transition at ~9 GPa: The phase transition (from IIb-2 to IIa-1, with space group C2/m unchanged) was evidenced in our high-pressure synchrotron XRD patterns (Fig. 2), which showed consistent with the recent high-pressure single-crystal XRD study (from IIb-4 to IIa-1) (Soldavini et al., 2024). Our results indicate that the IIa-1 prototype

could be a common high-pressure polytype regardless of whether the starting phase is triclinic (II*b*-4) or monoclinic (II*b*-2). According to the nomenclature proposed by Brown and Bailey (1962), the reorganization of the atoms consists of an a/3 translation of the brucite layer relative to the initial talc layer, changing from a *b*-type structure to an *a*-type (Soldavini et al., 2024). Moreover, we also found marked discontinuity in the pressure dependence of d_{002} spacing and c parameter at ~9 GPa (Fig. 3a & Fig. 4c). In contrast, d-spacing at high angles to the (001) plane, such as (33 $\overline{1}$), did not exhibit such discontinuous behaviour at ~9 GPa (Fig. 3b). This observation supports the results of Welch et al. (2004) and Kleppe et al. (2003) that the change of the structure predominantly involves the distortion along c-axis in the interlayer topology, manifesting as discontinuities in d_{002} spacing and c parameter.

Above 9 GPa, a discontinuity is observed in the pressure dependence of the interlayer OH modes, indicating significant changes in the OH-bonding environment. Notably, the vibration of (SiAl)O···O-H stretching mode disappeared (Fig. 5b), indicating the potential dehydroxylation of clinochlore. The observed positive frequency shifting rate of both 3572 cm⁻¹ and 3659 cm⁻¹ mode is approximately 20 cm⁻¹ GPa⁻¹, which is characteristic for (nearly) unbonded hydroxyl groups (Kleppe et al., 2003). Moreover, the bulk modulus of the high-pressure phase (IIa-1) shows a significant decrease of approximately 40% (Table 2), indicating the increasing compressibility of the structure. This reduction may be linked to partial dehydroxylation under high pressure, which would reduce the number of interlayer hydrogen bonds, thereby weakening interlayer repulsion and increasing structural compressibility.

Consequently, we interpret the polytypic phase transition at around 9 GPa as a reorganization of the interlayer hydrogen bonding, potentially transitioning to a state of very weakly hydrogen-bonded (including multi-furcated hydrogen bonds) or non-hydrogen-bonded hydroxyls-bearing phase. A potential trigger for this transition could be the maximal approach of basal tetrahedral sheets toward the interlayer sheets as pressure increases, eventually reaching a limit where a fraction of interlayer OH bonds was released out of the structure under compression. It is unlikely that the observed transition is due to the breaking of Si-O, Al-O, or Mg-O bonds, given the reversibility of the phase transition upon decompression (Fig. S2 & Fig. S4).

Structural distortion at ~12 GPa: Although the XRD patterns of clinochlore show no change in the number of diffraction peaks, indicating that the overall crystallographic symmetry is preserved, noticeable variations occur in both the d-spacings and the vibration of hydroxyl groups. In particular, the compressibility along interlayer contraction, as reflected by the d_{002} spacing, markedly decreases (from 0.069 Å/GPa to 0.016 Å/GPa) (Fig. 3a). The d_{331} spacing that sensitive to contraction within the layer remains constant above 12 GPa (Fig. 3b). These observations indicates that the compressibility across and within the layers reaches its limit, suggesting a shift in the overall compressibility of the structure. As for the high-pressure behaviour of hydroxyl groups, the OH mode exhibits a distinct shift rate of approximately 1.5 cm⁻¹·GPa⁻¹ to higher frequencies above ~12 GPa (Fig. 6b). Such positive pressure dependencies of OH-stretching frequencies at high pressures, which are less common than negative dependencies, are typically associated with pressure-enhanced hydrogen bonding, leading to hydrogen bond shortening and hydroxyl bond lengthening (He et al., 2024). Significant positive pressure-induced frequency shifts were explained by a combination of H-H repulsion and hydroxyl bond elongation toward an empty polyhedron (Lin et al., 2000). In the case of clinochlore, the high OH-stretching frequencies observed can likely be attributed to a combination of factors, including repulsion between anions and cations (O-O, neighbouring Si-H, and (Mg,Al)-H interactions), along with pressure-induced changes in the hydrogen bond properties.

Based on the above interpretations, we proposed that the structural distortion around 12 GPa is driven to the decreasing distance between layers, which leads to the formation of hydrogen bonds between the hydroxyl groups and oxygen of the sheets, increasing the repulsive forces between layers. Additionally, the IIa-phase shows the highest cation-cation repulsion between the tetrahedra of the TOT layer and the B layer among the other polytypes (Bailey, 1988), which leads to the nearly constant d_{331} spacing above 12 GPa. Overall, these factors contribute to the decreased compressibility observed beyond ~12 GPa.

It should be noted that we did not observe the discontinuity in OH-stretching frequencies within the 650–800 cm⁻¹ range at ~16 GPa, as reported by Kleppe et al. (2003). This discrepancy is likely due to variations in chemical composition, particularly the Mg/Fe ratio of the chlorite samples. The chlorite studied by Kleppe et al. (2003) was a pure Mg

end-member, containing no iron. In contrast, the chlorite sample in this study has an Mg/Fe ratio of approximately 1.8, exhibiting a phase transition pressure in the ranges of 9-10 GPa. Our observation is supported by Soldavini et al. (2024), reporting a similar phenomenon with a Mg/Fe ratio of ~1.7. Atomically, although Fe²⁺ and Mg²⁺ are isovalent and possess similar ionic radii, differences in cation composition can induce subtle local structural distortions, alter hydrogen-bonding geometries, and modify the size of octahedral sites. These factors may influence how hydroxyl groups respond to compression, particularly in terms of vibrational frequency shifts and hydrogen bond strength. Other factors, such as pressure calibration uncertainties and minor chemical heterogeneities in natural samples may also contribute to these differences.

Overall, the high-pressure behaviour of chlorite is complex and likely influenced by multiple interacting variables. To further clarify the role of compositional variability, additional high-pressure studies on chlorite samples with varying chemical compositions are needed, particularly those incorporating high-pressure neutron diffraction which can directly probe hydrogen positions and bonding environments.

Conclusions

X-ray diffraction and infrared spectroscopy were employed to study the high-pressure structural behaviour of clinochlore. Polytypic phase transition and structural distortion were found at ~9 GPa and ~12 GPa, respectively. The polytypic phase transition around 9 GPa was marked by the reorganization of interlayer hydrogen bonding, potentially transitioning to a state of very weakly bonded or non-hydrogen-bonded hydroxyl groups. The distortion near 12 GPa involves a more complex behaviour in the hydroxyl groups and metal-oxygen sublattice, which may relate to the compression limits of interlayer distances and subsequent changes in hydrogen bonding patterns. These findings significantly contribute to our understanding of the structural behaviour of chlorite at high pressures. To advance the geodynamic implications of chlorite, further studies are needed to investigate the structural evolution and dehydration behavior under high-pressure and high-temperature conditions relevant to the Earth's interior, with the aim of more accurately evaluating its potential role in transporting water into the deep mantle.

Acknowledgments

We greatly thank the editor and anonymous referees for their effort and careful reviews of this manuscript. This research was supported by the National Science and Technology Major Project of the Ministry of Science and Technology of China (Grants Nos. 2025ZD1010301 to B.X.H.) and the National Natural Science Foundation of China (Grants Nos. 42272047 to H.Y.Z. and 42102034 to J.J.N.) and the China Postdoctoral Science Foundation (Grants Nos.

2 0 1 9 M 6 6 0 8 1 6 to J. J. N.)

Competing interests

The authors declare no competing interests.

References

- Bailey, S. (1988). Hydrous Phyllosilcates. Mineralogical Society of America. *Reviews in Mineralogy*, 19, 347–398.
- Birch, F. (1947). Finite elastic strain of cubic crystals. *Physical Review*, 71(11), 809.
- Brown, B. t., & Bailey, S. (1962). Chlorite polytypism: I. Regular and semi-random one-layer structures. *American Mineralogist: Journal of Earth and Planetary Materials*, 47(7–8), 819–850.
- Fumagalli, P., & Poli, S. (2005). Experimentally determined phase relations in hydrous peridotites to 6.5 GPa and their consequences on the dynamics of subduction zones. *Journal of Petrology*, 46(3), 555–578.
- Gonzalez-Platas, J., Alvaro, M., Nestola, F., & Angel, R. (2016). EosFit7-GUI: a new graphical user interface for equation of state calculations, analyses and teaching. *Journal of Applied Crystallography*, 49(4), 1377–1382.
- Grevemeyer, I., Ranero, C. R., & Ivandic, M. (2018). Structure of oceanic crust and serpentinization at subduction trenches. *Geosphere*, 14(2), 395–418.
- He, X., Kagi, H., Komatsu, K., Sano-Furukawa, A., Abe, J., Fukuyama, K., Shinmei, T., & Nakano, S. (2024) High-pressure behaviors of hydrogen bonds in fluorine-doped brucite. *Inorganic Chemistry*, 63(47), 22349–22360.
- Hermann, J., & Lakey, S. (2021). Water transfer to the deep mantle through hydrous, Al-rich silicates in subduction zones. *Geology*, 49(8), 911–915.
- Jenkins, D. M. (1981). Experimental phase relations of hydrous peridotites modelled in the system H₂O-CaO-MgO-Al₂O₃-SiO₂. *Contributions to Mineralogy and Petrology*, 77, 166–176.
- Kim, D., Jung, H., & Lee, J. (2023). Impact of chlorite dehydration on intermediate-depth earthquakes in subducting slabs. *Communications Earth & Environment*, 4(1), 491.
- Kleppe, A. K., Jephcoat, A. P., & Welch, M. D. (2003). The effect of pressure upon hydrogen bonding in chlorite: a Raman spectroscopic study of clinochlore to 26.5 GPa. *American Mineralogist*, 88(4), 567–573.
- Kloprogge, J. T., & Frost, R. L. (2000). Thermal decomposition of Ferrian chamosite: an infrared emission spectroscopic study. *Contributions to Mineralogy and Petrology*,

- *138*(1), 59–67.
- Lin, C.-C., Liu, L.-G., Mernagh, T., & Irifune, T. (2000). Raman spectroscopic study of hydroxyl-clinohumite at various pressures and temperatures. *Physics and Chemistry of Minerals*, 27, 320–331.
- Mao, H., Xu, J.-A., & Bell, P. (1986). Calibration of the ruby pressure gauge to 800 kbar under quasi-hydrostatic conditions. *Journal of Geophysical Research: Solid Earth*, 91(B5), 4673–4676.
- Peacock, S. M. (1990). Fluid processes in subduction zones. Science, 248(4953), 329–337.
- Prescher, C., & Prakapenka, V. B. (2015). DIOPTAS: a program for reduction of two-dimensional X-ray diffraction data and data exploration. *High Pressure Research*, 35(3), 223–230.
- Prieto, A., Dubessy, J., & Cathelineau, M. (1991). Structure-composition relationships in trioctahedral chlorites: a vibrational spectroscopy study. *Clays and Clay Minerals*, 39(5), 531–539.
- Rietveld, H. M. (1969). A profile refinement method for nuclear and magnetic structures. *Applied Crystallography*, 2(2), 65–71.
- Schmidt, M. W., & Poli, S. (1998). Experimentally based water budgets for dehydrating slabs and consequences for arc magma generation. *Earth and Planetary Science Letters*, 163(1–4), 361–379.
- Serratosa, J., & Vinas, J. (1964). Infra-red Investigation of the OH Bonds in Chlorites. *Nature*, 202(4936), 999.
- Shirozu, H. (1980). Cation distribution, sheet thickness, and O-OH space in trioctahedral chlorites—an X-ray and infrared study. *Mineralogical Journal*, 10(1), 14–34.
- Soldavini, B. C., Comboni, D., Hanfland, M., & Merlini, M. (2024). High-pressure phase transition in clinochlore: IIa polytype stabilization. *American Mineralogist*, 109(10), 1834-1838.
- Till, C. B., Grove, T. L., & Withers, A. C. (2012). The beginnings of hydrous mantle wedge melting. *Contributions to Mineralogy and Petrology, 163*, 669–688.
- Toby, B. H. (2001). EXPGUI, a graphical user interface for GSAS. *Journal of Applied Crystallography*, 34(2), 210–213.
- Velde, B. (1980). Ordering in synthetic aluminous serpentines; infrared spectra and cell dimensions. *Physics and Chemistry of Minerals*, 6(3), 209–220.
- Welch, M. D., Barras, J., & Klinowski, J. (1995). A multinuclear NMR study of clinochlore. *American Mineralogist*, 80(5–6), 441–447.
- Welch, M. D., Kleppe, A. K., & Jephcoat, A. P. (2004). Novel high-pressure behavior in chlorite: A synchrotron XRD study of clinochlore to 27 GPa. *American Mineralogist*, 89(8–9), 1337–1340.
- Welch, M. D., & Marshall, W. G. (2001). High-pressure behavior of clinochlore. *American Mineralogist*, 86(11–12), 1380–1386.
- Yang, M., Ye, M., Han, H., Ren, G., Han, L., & Zhang, Z. (2018). Near-Infrared Spectroscopic Study of Chlorite Minerals. *Journal of Spectroscopy*, 2018, 1–11.

Zanazzi, P. F., Montagnoli, M., Nazzareni, S., & Comodi, P. (2006). Structural effects of pressure on triclinic chlorite: A single-crystal study. *American Mineralogist*, 91(11–12), 1871–1878.

Zanazzi, P. F., Montagnoli, M., Nazzareni, S., & Comodi, P. (2007). Structural effects of pressure on monoclinic chlorite: A single-crystal study. *American Mineralogist*, 92(4), 655–661.

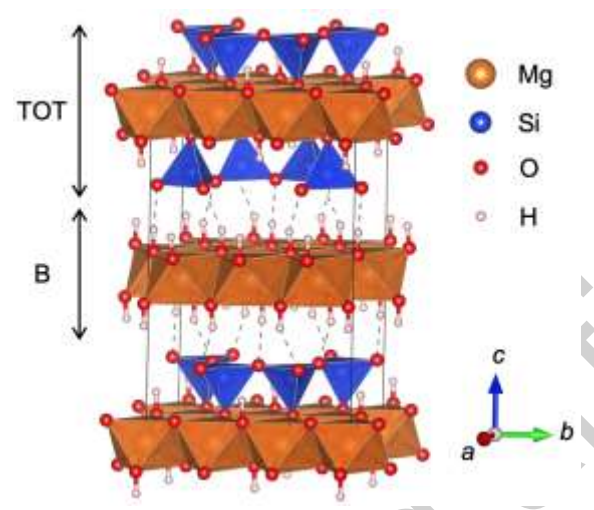


Fig. 1 The structure of monoclinic C2/m clinochlore. Brucite-like (B) layers and talc-like (TOT) layers are connected by hydrogen bonds (dashed lines). Other cations (e.g. Al, Fe) are not shown for similarity.

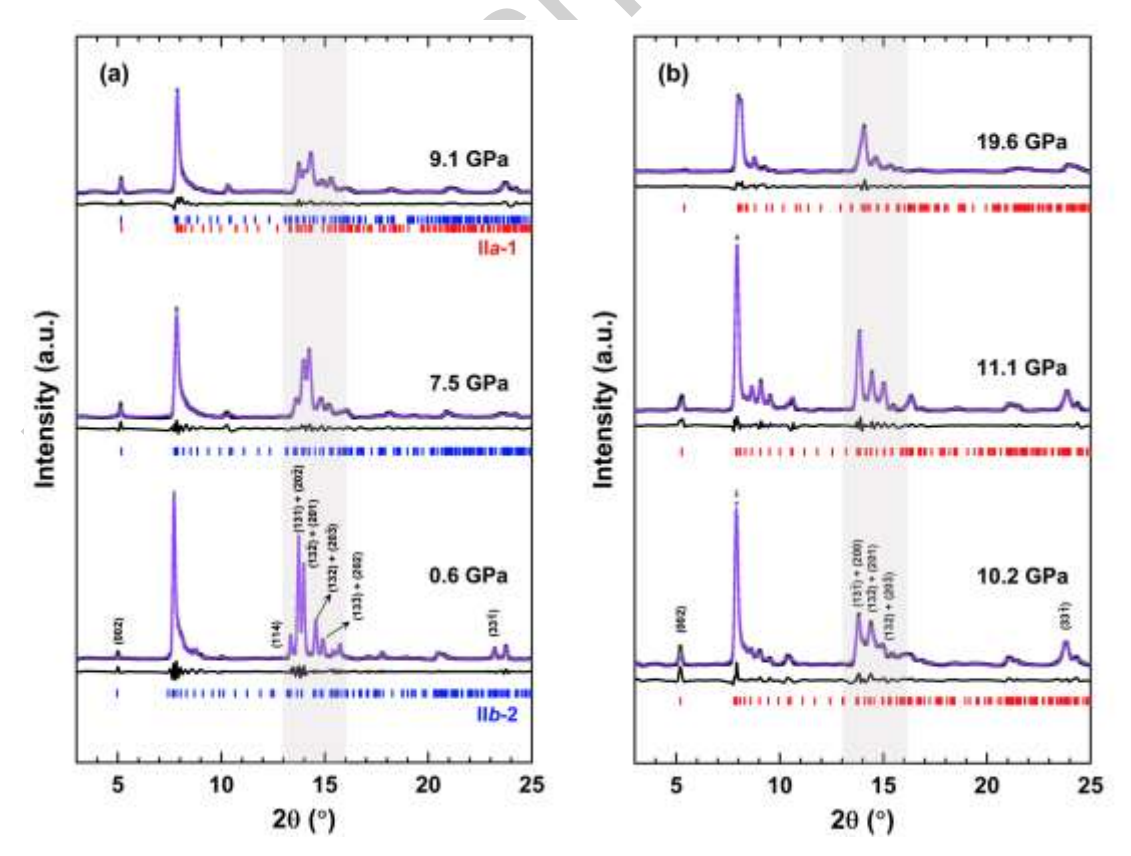


Fig. 2 Selected X-ray diffraction patterns of (a) II*b*-2 type clinochlore and (b) II*a*-1 type clinochlore at high pressures. Rietveld refinements (purple curves) of observed XRD data (black dots) were carried out after background subtraction. The grey box highlights the 2θ range of $13-16^{\circ}$ (d=2.74-2.23 Å).

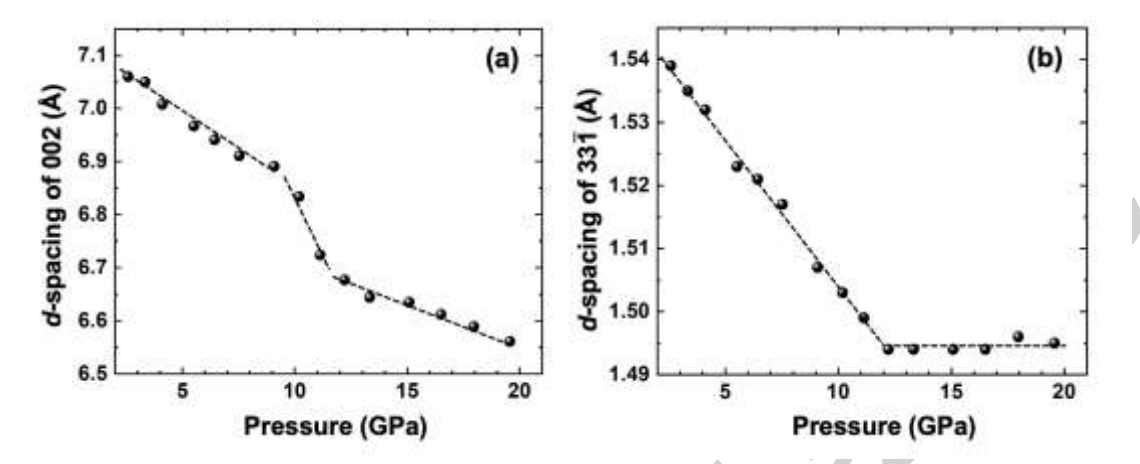


Fig. 3 Variation of d-spacings of key reflections (a) d_{002} and (b) $d_{33\overline{1}}$. Dashed lines represent the linear pressure dependence of d-spacings.

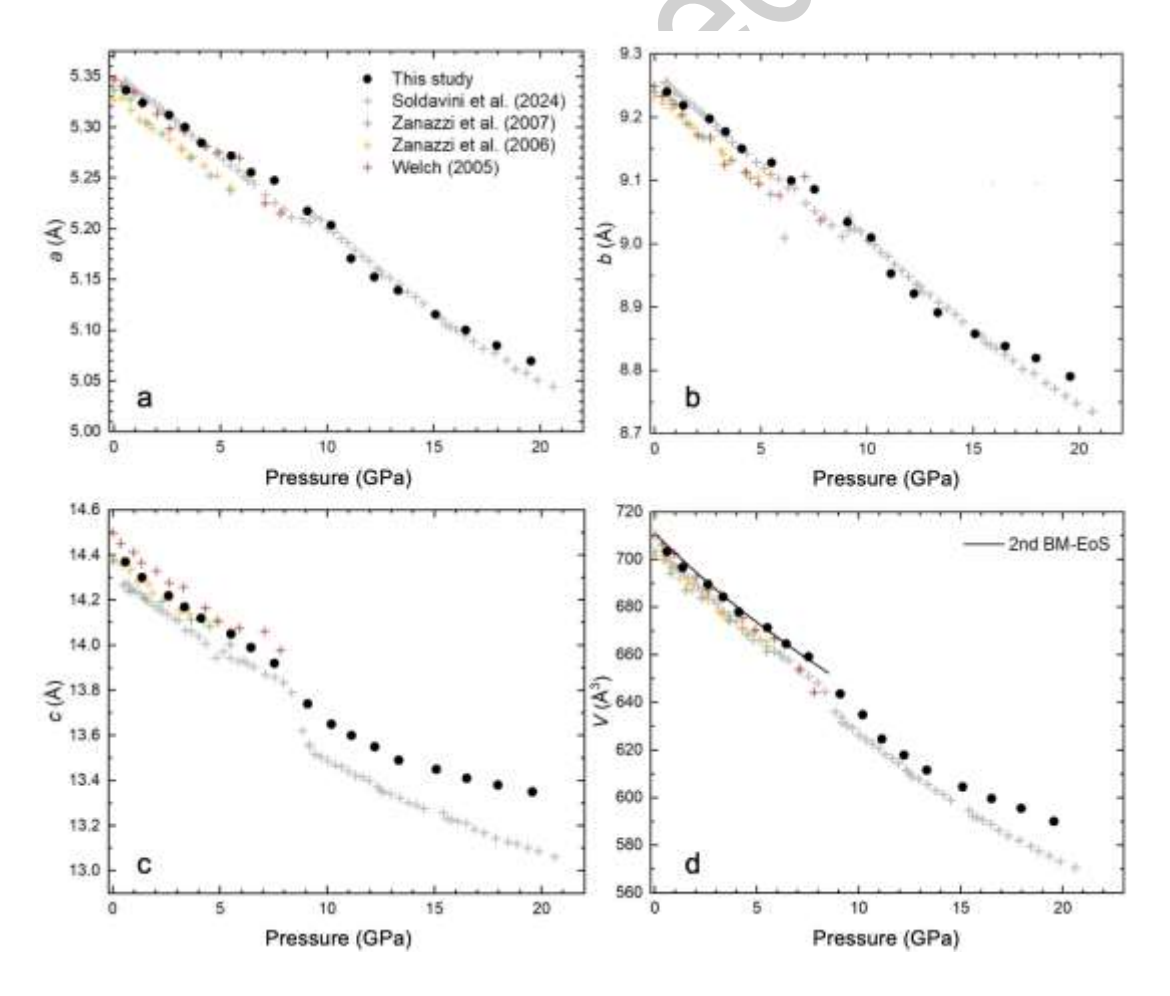


Fig. 4 Unit-cell parameters for clinochlore as a function of pressure compared with previous studies. (a)&(b)&(c) Variations of structural parameters of a, b, c with pressure. Discontinuity is observed at ~9 GPa, which shows good agreement with previous results. (d) The unit-cell volume as a function of pressure. The volume data of low-pressure structure (< 9 Gpa) of clinochlore is fitted to second-order Birch-Murnaghan equations of state for which $V_0 = 710.9(3) \text{ Å}^3$ and $K_0 = 83.4(8)$ GPa.

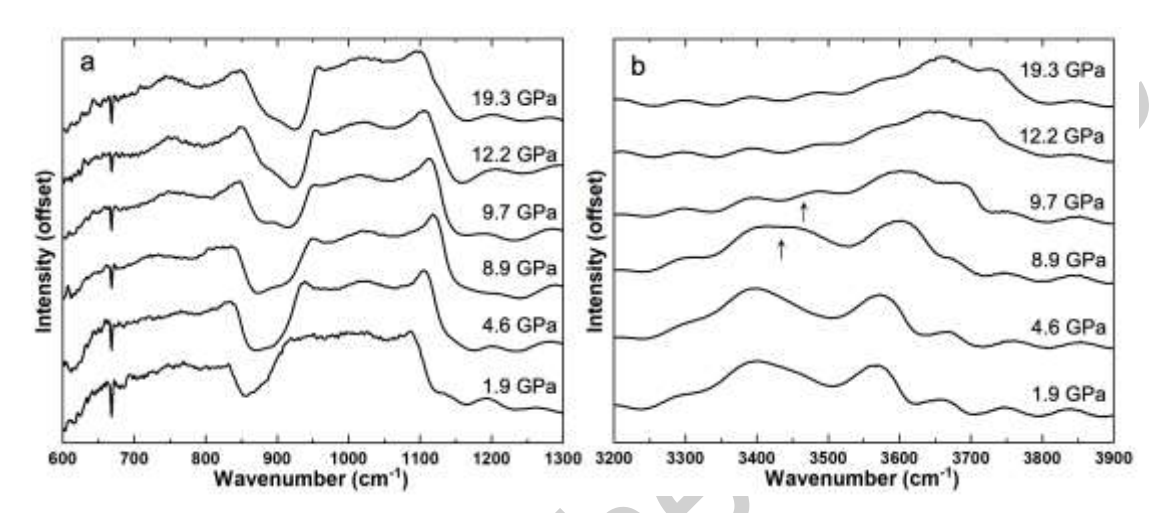


Fig. 5 Representative IR spectra of clinochlore as a function of pressure in 600–1100 cm⁻¹ region (a) and OH-stretching frequency in 3300–3700 cm⁻¹ region (b). The black arrows indicate the disappearing of the 3407 cm⁻¹ vibration mode.

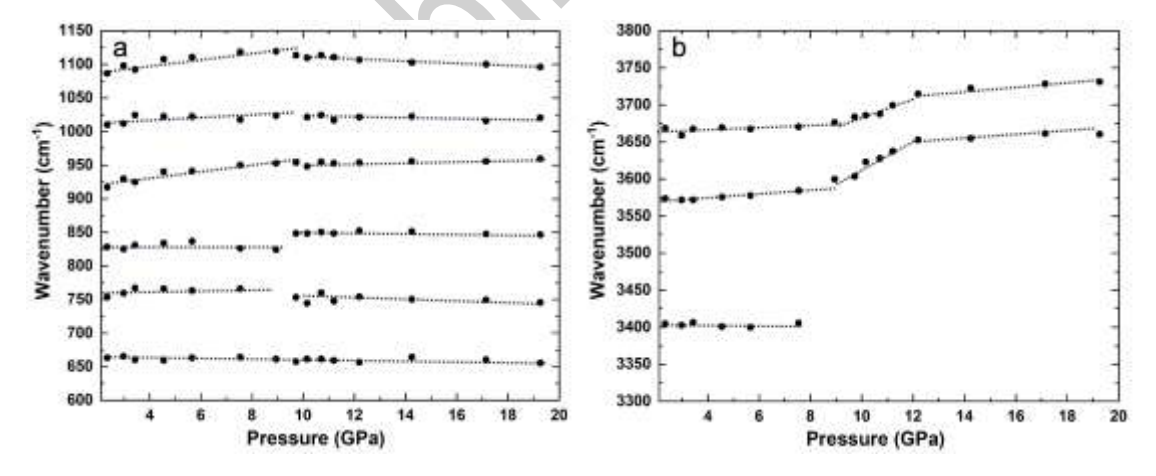


Fig. 6 Pressure dependence of the stretching modes of clinochlore in 600–1100 cm⁻¹ region (a) and OH-stretching frequency in 3300–3700 cm⁻¹ region (b). Dashed lines represent the linear pressure dependence of modes.

Table 1. Variations of lattice parameters and key d-spacings of clinochlore with pressure

Step	P (GPa)	a (Å)	b (Å)	c (Å)	β(°)	$V(\mathring{A}^3)$	d_{002} (Å)	d_{331} (Å)
II <i>b</i> -2								
1	0.6	5.34(1)	9.24(3)	14.37(3)	96.99(1)	703.29(4)	7.097	1.540
2	1.4	5.32(2)	9.22(1)	14.30(1)	96.93(1)	696.69(6)	7.097	1.539
3	2.6	5.31(1)	9.20(3)	14.22(3)	96.92(1)	689.69(8)	7.060	1.539
4	3.3	5.30(3)	9.18(1)	14.17(1)	96.87(1)	684.30(1)	7.050	1.535
5	4.1	5.28(1)	9.15(3)	14.12(2)	96.76(1)	678.02(4)	7.008	1.532
6	5.5	5.27(1)	9.13(2)	14.05(3)	96.75(1)	671.41(6)	6.967	1.523
7	6.4	5.26(1)	9.10(2)	13.99(1)	96.60(1)	664.63(4)	6.941	1.521
8	7.5	5.25(1)	9.09(1)	13.92(3)	96.65(1)	659.24(8)	6.911	1.517
II <i>a</i> -1	9.1	5.22(3)	9.03(1)	13.74(1)	97.11(1)	643.58(1)	6.891	1.507
9	10.2	5.20(2)	9.01(3)	13.65(3)	97.21(1)	634.87(4)	6.834	1.503
10	11.1	5.17(1)	8.95(3)	13.60(1)	97.15(2)	624.66(1)	6.724	1.499
11	12.2	5.15(3)	8.92(2)	13.55(2)	97.23(1)	617.88(3)	6.677	1.494
12	13.3	5.14(1)	8.89(1)	13.49(1)	97.18(3)	611.56(2)	6.644	1.494
13	15.1	5.12(2)	8.86(2)	13.45(1)	97.24(2)	604.58(4)	6.635	1.494
14	16.5	5.10(3)	8.84(1)	13.41(3)	97.22(1)	599.68(3)	6.612	1.494
15	18.0	5.08(2)	8.82(1)	13.38(2)	96.98(1)	595.56(2)	6.589	1.496
16	19.6	5.07(1)	8.79(1)	13.35(1)	97.30(1)	590.09(4)	6.561	1.495
17	J.							

Table 2. BM-EoS parameters of chlorite comparing with previous results

V_0 (Å ³)	K_0 (GPa)	K_1	Polytype	Reference
710.9(3)	83.4(8)	4	II <i>b</i> -2	This study
-	81.2(13)	4	II <i>b</i> -4	Soldavini et
				al., 2024
718.0(10)	56.0(6)	4	II <i>a</i> -1	Soldavini et
				al., 2024
703.2(8)	71(9)	8(5)	II <i>b</i> -2	Zanazzi et al.,
				2007
701.8(1)	88(5)	5(3)	II <i>b</i> -4	Zanazzi et al.,
				2006
710.32(28)	78.7(14)	4	I <i>a</i> -4	Welch and
				Crichton 2005
-	81	4	Πb	Welch and
		M		Crichton 2005